

Nucleosynthesis of ^{56}Ni in wind-driven Supernova Explosions and Constraints on the Central Engine of Gamma-Ray Bursts

Keiichi Maeda^{1*} and Nozomu Tominaga²

¹*Institute for the Physics and Mathematics of the Universe (IPMU), University of Tokyo, Kashiwanoha 5-1-5, Kashiwa-shi, Chiba 277-8568, Japan*

²*Division of Optical and Infrared Astronomy, National Astronomical Observatory of Japan, 2-21-1 Osawa, Mitaka, Tokyo 181-8588, Japan*

ABSTRACT

Theoretically expected natures of a supernova driven by a wind/jet are discussed. Approximate analytical formulations are derived to clarify basic physical processes involved in the wind/jet-driven explosions, and it is shown that the explosion properties are characterized by the energy injection rate (\dot{E}_{iso}) and the mass injection rate (\dot{M}_{iso}). To explain observations of SN 1998bw associated with Gamma-Ray Burst (GRB) 980425, the following conditions are required: $\dot{E}_{\text{iso}}\dot{M}_{\text{iso}} \gtrsim 10^{51} \text{ erg } M_{\odot} \text{ s}^{-2}$ and $\dot{E}_{\text{iso}} \gtrsim 2 \times 10^{52} \text{ erg s}^{-1}$ (if the wind Lorentz factor $\Gamma_{\text{w}} \sim 1$) or $\dot{E}_{\text{iso}} \gtrsim 7 \times 10^{52} \text{ erg s}^{-1}$ (if $\Gamma_{\text{w}} \gg 1$). In SN 1998bw, ^{56}Ni ($\sim 0.4M_{\odot}$) is probably produced in the shocked stellar mantle, not in the wind. The expected natures of SNe, e.g., ejected ^{56}Ni masses and ejecta masses, vary depending on \dot{E}_{iso} and \dot{M}_{iso} . The sequence of the SN properties from high \dot{E}_{iso} and \dot{M}_{iso} to low \dot{E}_{iso} and \dot{M}_{iso} is the following: SN 1998bw-like – intermediate case – low mass ejecta ($\lesssim 1M_{\odot}$) where ^{56}Ni is from the wind – whole collapse. This diversity may explain the diversity of supernovae associated with GRBs. Our result can be used to constrain natures of the wind/jet, which is linked to the central engine of GRBs, by studying properties of the associated supernovae.

Key words: gamma-ray: bursts – supernovae: general – supernovae: individual (SN 1998bw) – nuclear reactions, nucleosynthesis, abundances.

1 INTRODUCTION

Gamma-Ray Bursts (GRBs) are energetic cosmological events, emitting $\gtrsim 10^{51}$ ergs in γ -ray. A leading model for the central engine of GRBs is the formation of a black hole (BH) and an accretion disk, following the gravitational collapse of a massive star whose main sequence mass (M_{ms}) is at least as large as $25M_{\odot}$ (for reviews, see Woosley & Bloom 2006; Nomoto et al. 2007). A relativistic flow generated by neutrino annihilation (Woosley 1993; MacFadyen & Woosley 1999) or magnetic activity (Brown et al. 2000; Proga et al. 2003) is proposed to trigger a GRB.

A link between (a class of) GRBs and Type Ic supernovae (SNe Ic) has been established observationally. The most convincing cases for the supernovae associated with GRBs (hereafter GRB-SNe) have been provided by spectroscopic detection of supernova features in an optical afterglow of a GRB or at the position consistent with a GRB. Three

nearby GRB-SNe detected in this way are found to be similar to one another. The category includes GRB 980425/SN 1998bw (the proto-typical GRB-SN; Galama et al. 1998), GRB 030329/SN 2003dh (Hjorth et al. 2003; Kawabata et al. 2003; Matheson et al. 2003; Stanek et al. 2003), and GRB 031203/SN 2003lw (Malesani et al. 2004; Thomsen et al. 2004). Optical observations of these GRB-SNe are well explained by an explosion of a carbon-oxygen (CO) star, which has evolved from a massive star ($M_{\text{ms}} \sim 40M_{\odot}$) and has lost its H- and He-envelopes during the hydrostatic evolutionary phase (Iwamoto et al. 1998; Woosley et al. 1999; Nakamura et al. 2001a; Mazzali et al. 2003, 2006). The kinetic energy (E_{K}) of the expansion is large, $E_{51} \equiv E_{\text{K}}/10^{51}$ ergs $\gtrsim 10$ (note that $E_{51} \sim 1$ for canonical supernovae). They eject $\sim 0.3 - 0.7M_{\odot}$ of ^{56}Ni (which powers the SN luminosity by the decay chain $^{56}\text{Ni} \rightarrow \text{Co} \rightarrow \text{Fe}$). Hereafter, the mass of ^{56}Ni is denoted by $M(^{56}\text{Ni})$. Recently, another example of the association has been reported (Della Valle et al. 2008; Soderberg et al. 2008), i.e., GRB 081007/SN Ic

* E-mail: keiichi.maeda@ipmu.jp

2008hw, while the observed properties of this SN have not been modeled yet.

Despite the similarity within the well studied cases mentioned above, GRB-SNe do seem to have diverse properties. Peak magnitudes of so-called supernova bumps seen in GRB optical afterglows show diversity (Zeh, Klose, & Hartmann 2004; Woosley & Bloom 2006), highlighted by sub-luminous (possible) SNe in GRBs 040924 and 041006 (Soderberg et al. 2006). A few GRBs show no evidence for the supernova bump (Hjorth et al. 2000; Price et al. 2003). Non-detection of SN features in two nearby GRBs 060505 and 060614 has been reported, placing the upper limit to brightness of possible underlying SNe ~ 100 times fainter than SN 1998bw (Della Valle et al. 2006; Fynbo et al. 2006; Gal-Yam et al. 2006).

In spite of the observational constraints, the explosion mechanism of GRBs and GRB-SNe are still unknown. In particular, how properties of the central engine are related to the bulk expansion of the stellar materials, observed as a supernova mainly in visual light, is still under debate. A possibility is that a supernova is induced by a disk wind generated by viscous heating (MacFadyen & Woosley 1999; Narayan, Piran, & Kumar 2001).

Although there were numerical calculations for the wind/jet-driven explosions (Khokhlov et al. 1999; MacFadyen, Woosley, & Heger 2001; Maeda & Nomoto 2003; Nagataki et al. 2003; Maeda 2004; Nagataki, Mizuta, & Sato 2006; Tominaga 2007a; Tominaga et al. 2007b; and Tominaga 2009), it has not been clarified what fundamentally determines the properties of resulting SNe and in what ways. Also, the numerical investigations have been restricted in the parameter space.

Aiming to overcome these problems, this study is complementary to the past numerical studies. Our goal in this paper is to express theoretically expected features of SNe resulting from the wind/jet-driven explosion, as a function of rates of the mass and energy (\dot{M}_w and \dot{E}_w , where the subscript "w" denotes "wind", or \dot{M}_{iso} and \dot{E}_{iso} , referring to the isotropic equivalent values) generated and injected from the central system (i.e., a black hole plus a disk) into the surrounding stellar mantle (in this paper, stellar "mantle" refers to the stellar materials above the central remnant, i.e., the outermost layer of the Fe core, and the Si- and CO-layers).

Our strategy is the following. (1) We first clarify what are main ingredients of the wind/jet-driven SN explosion (§2). We develop a simplified description for the shock propagation and nucleosynthesis in the explosion (§3). We especially focus on the production of ^{56}Ni , addressing how two proposed sites for the ^{56}Ni production, a shocked stellar mantle and a disk wind (MacFadyen & Woosley 1999; see Maeda & Nomoto 2003 for a review), can be distinguished. (2) We then compare the results with observations of SNe associated with a GRB, in order to constrain \dot{M}_{iso} and \dot{E}_{iso} in these SNe (§4). The required values for \dot{M}_{iso} and E_{iso} then should be regarded as conditions that any models for the central engine should satisfy. In other word, by constraining \dot{M}_{iso} and \dot{E}_{iso} , we aim to provide useful constraints in studying the properties of the central engine of GRBs.

2 MODELS

We consider a situation that a supernova explosion is driven by outflow of materials (e.g., a disk wind; MacFadyen & Woosley 1999) from the vicinity of a central remnant (likely a black hole). This energy input can be different from the relativistic jet producing a GRB; The wind can either be relativistic or non-relativistic at its injection from the central remnant into the surrounding stellar mantle.

A schematic picture of the problem considered in this paper (and most of the past numerical studies) is shown in Figure 1. Throughout this paper, we adopt $25M_{\odot}$ and $40M_{\odot}$ progenitor models from Nomoto & Hashimoto (1988). Following the treatment of the past numerical studies, the wind/jet (we hereafter frequently call it simply a wind) is injected by hand at a certain radius (R_w in this paper).

2.1 Properties of the wind/jet

In a one-dimensional hydrodynamic problem, three independent variables must be specified (two for thermodynamic variables and one for a hydrodynamic variable) as initial/boundary conditions. For simplicity, we assume that the wind is dominated by the kinetic energy. This does not drastically defeat our results, since it is expected that the thermal energy deposited at the root of the wind, near the central remnant, is quickly converted to the kinetic energy well below R_w . Thanks to this simplification, only two independent variables at R_w are required to determine the hydrodynamic evolution of the system. The choice of the independent variables can be arbitrary, thus we take the energy injection rate (\dot{E}_w) and the mass injection rate (\dot{M}_w). The Lorentz factor of the wind/jet at the injection (at R_w) is expressed as a function of these two independent variables, i.e., $\Gamma_w \sim 1 + \dot{E}_w / (\dot{M}_w c^2)$, where c is the speed of light. Hereafter, quantities expressing the properties of the wind at injection (at R_w) are denoted by the subscript "w". Trivially, the wind is initially highly relativistic only if $\dot{E}_{w,51} / \dot{M}_{w,\odot} \gg 1000$, where $\dot{E}_{w,51} \equiv \dot{E}_w / (10^{51} \text{ erg s}^{-1})$ and $\dot{M}_{w,\odot} \equiv \dot{M}_w / (M_{\odot} \text{ s}^{-1})$.

Our analysis is based on a one-dimensional radial flow; The collimation of the wind is taken into account with a geometrical factor $f_{\Omega} (\leq 1)$. f_{Ω} relates the wind intrinsic properties and isotropic equivalents as

$$\dot{E}_w = f_{\Omega} \dot{E}_{\text{iso}}, \quad (1)$$

$$\dot{M}_w = f_{\Omega} \dot{M}_{\text{iso}}, \quad (2)$$

$$E_w = f_{\Omega} E_{\text{iso}}, \quad (3)$$

where E_w is the intrinsic total energy (i.e., the injected energy integrated over time), and the subscript "iso" refers to isotropic equivalent values. f_{Ω} is a measure of the collimation angle of the wind at R_w : When the wind is a spherically symmetric flow, $f_{\Omega} = 1$. The wind is more narrowly collimated at the injection for smaller f_{Ω} .

For the temporal history of the wind properties, we focus on the situation that the wind is injected at R_w , with \dot{E}_w and \dot{M}_w constant in time for $t < t_w$, and then terminated at $t = t_w$, so that

$$E_w = \dot{E}_w t_w \text{ (or equivalently, } E_{\text{iso}} = \dot{E}_{\text{iso}} t_w \text{)}. \quad (4)$$

Some of the following results, however, do not rely on this assumption.

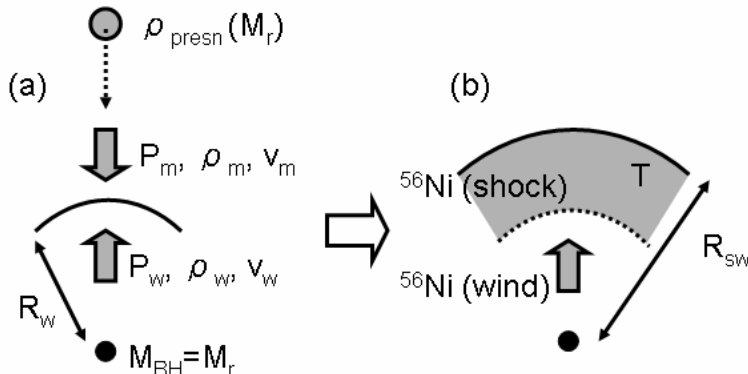


Figure 1. A schematic picture of a wind/jet-driven SN explosion. (a) A situation before the launch of the outward shock wave. The wind/jet is assumed to be continuously injected from the central remnant with properties denoted by the subscript "w" at radius R_w . When materials initially at M_r in the presupernova progenitor fall to R_w , their properties are denoted by the subscript "m". At this point, the mass of the central remnant (the mass within R_w) is M_r . (b) A situation after the launch of the outward shock wave. The shock wave arrives at radius R_{sw} , and temperature behind the shock is denoted by T . ^{56}Ni is produced both in the shocked stellar materials between R_{sw} and R_w and within the wind/jet itself.

2.2 Processes involved

2.2.1 Collapse to Explosion

The first function we have to consider is the dynamical effect (§3.1) of the wind to the collapsing stellar mantle; the overlying stellar mantle continues to collapse onto the central remnant, and the wind does not always have a sufficiently large momentum to overcome the ram pressure of the infalling materials (Fig. 1a). The importance of the dynamical effect to determine the outcome of a wind/jet-driven supernova explosion was pointed out by Maeda (2004) and numerically examined by Maeda (2004) and Tominaga et al. (2007b). Some numerical calculations have included the dynamical effect self-consistently (e.g., Maeda & Nomoto 2003; Maeda 2004; Tominaga et al. 2007b; Tominaga 2009), while others have not (e.g., Maeda et al. 2002; Nagataki et al. 2003).

2.2.2 Production of ^{56}Ni

Once the shock wave is launched, it propagates outward into the stellar mantle (Fig. 1b). The kinetic energy is now converted to the thermal energy following the shock wave propagation. The temperature behind the shock wave is initially so high that the nuclear burning converts the initial stellar composition (mostly oxygen and silicon) mainly to ^{56}Ni (§3.2.1). The temperature decreases as the shock wave moves outward; once the temperatures drops below $\sim 5 \times 10^9$ K, then the efficiency of the production of ^{56}Ni decreases rapidly.

At the same time, the temperature of the injected wind itself may also be sufficiently high so that a fraction of this material may be converted to ^{56}Ni (§3.2.2). In most of the past numerical studies, the production of ^{56}Ni in shocked stellar mantle has been investigated in detail. The ejection of ^{56}Ni in the wind has been examined by a different kind of numerical simulations involving the innermost part of the collapsing star (e.g., MacFadyen & Woosley 1999; Nagataki et al. 2007). However, in such simulations, it is practically

difficult to follow the dynamics of the shock wave propagating into the stellar mantle; Thus, it has not been yet clear how the amount of ^{56}Ni synthesized in the wind is connected to properties of the progenitor star and of the resulting supernova.

2.2.3 Geometry of the ejecta

Finally, the properties of the wind affect the shape of the supernova ejecta, as the shock wave propagates through the stellar mantle. This has been directly examined in the past numerical studies, but restricted in the parameter space. In this paper, we derive a simple estimate of the shape, in terms of the properties of the wind (§3.3).

3 WIND/JET-DRIVEN EXPLOSIONS

3.1 Collapse to Explosion

In this section, we examine dynamical effect of the wind on the collapsing stellar mantle (Fig. 1a). We follow analysis similar to that given by Fryer & Mészáros (2003) for a standard neutrino-driven delayed explosion for (canonical) supernovae.

We evaluate outcome of the interaction between the wind and the infalling materials at radius $R_w \sim 8 \times 10^7$ cm (for $M_{ms} = 40M_\odot$) and 1.2×10^8 cm ($M_{ms} = 25M_\odot$), where the presupernova enclosed mass (M_r) is $1.4M_\odot$. As time goes by, materials initially at larger M_r collapses to the radius R_w , and add to the mass of the central remnant (M_{BH}). During a whole period before the launch of the shock, the temporal evolution of the system is thus specified by the central remnant mass M_{BH} which monotonically increases as a function of time (i.e., larger M_{BH} for later time).

If the trajectory of the infalling materials is that of free fall, the density (ρ_m) and velocity (v_m) of the infalling ma-

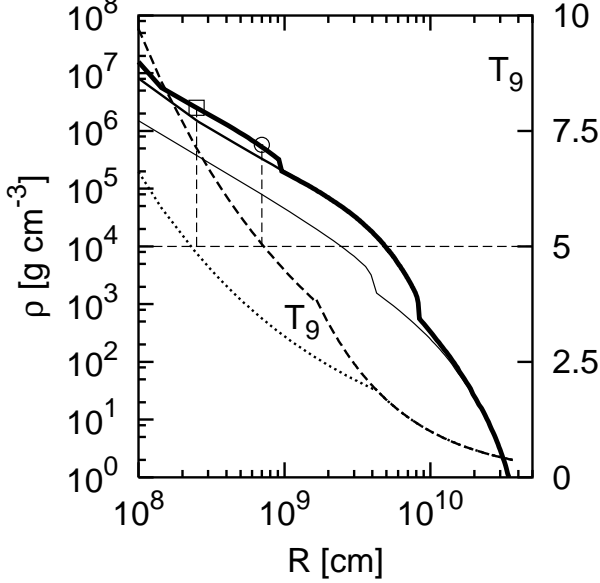


Figure 2. Density Structure (left vertical axis label) following the gravitational collapse, at $M_{\text{BH}} = 2.4M_{\odot}$ (thick-solid line), $3.4M_{\odot}$ (medium-solid), and $13M_{\odot}$ (thin-solid). Also shown is the postshock temperature ($T_9 \equiv T/10^9$ K; right vertical axis label) as a function of the shock radius, for $M_{\text{BH}} = 2.4M_{\odot}$, $\dot{E}_{\text{iso},51} = 30$, and $\dot{E}_{\text{iso},51} = 10$ (dashed line) or 1 (dotted line). The progenitor model ($M_{\text{ms}} = 40M_{\odot}$) is from Nomoto & Hashimoto (1988). The position within which the postshock temperature is above 5×10^9 K (horizontal thin-dashed line), for $M_{\text{BH}} = 2.4M_{\odot}$, is marked by the open circle ($\dot{E}_{\text{iso},51} = 10$) and by the open square ($\dot{E}_{\text{iso},51} = 1$).

terials at R_w are written as

$$\rho_m \sim \rho_{\text{presn}} \left(\frac{R_{\text{presn}}}{R_w} \right)^{3/2}, \quad (5)$$

$$v_m \sim \left(\frac{2GM_r}{R_w} \right)^{1/2}. \quad (6)$$

The subscript "presn" is used for the pre-collapse initial values for the material at the mass coordinate M_r . The subscript "m" refers to quantities of the same material (at M_r) when it collapses to R_w (Figure 1a). Figure 2 shows snapshots of the density structure for different M_{BH} for $M_{\text{ms}} = 40M_{\odot}$.

The outward shock wave is launched if the ram pressure of the wind (P_w) overcomes that of the infalling materials (P_m), i.e.,

$$P_w \sim \Gamma_w^2 \rho_w v_w^2 \geq P_m = \rho_m v_m^2 \equiv \rho_m \bar{g} \frac{GM_{\text{BH}}}{R_w}. \quad (7)$$

Here M_{BH} is the mass of the BH when the material at M_r ($= M_{\text{BH}}$) collapses to R_w . Although a numerical constant $\bar{g} = 2$ in the above estimate, we find $\bar{g} = 1/2$ yields a better representation of a set of numerical simulations (Maeda 2004; Tominaga et al. 2007b). We assume $\bar{g} = 1/2$ throughout the paper.

Equation (7) can be expressed in terms of \dot{E}_w and \dot{M}_w , which are related to other properties of the wind/jet as fol-

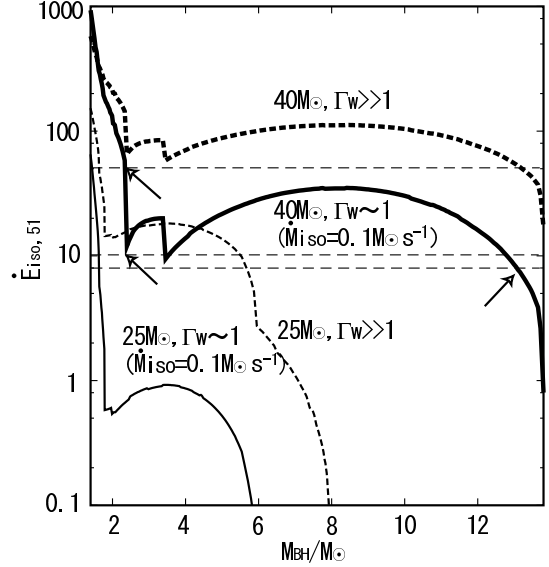


Figure 3. The requirement for \dot{E}_{iso} to initiate the explosion as a function of M_{BH} . For $\Gamma_w \sim 1$, the case with $\dot{M}_{\text{iso}} = 0.1M_{\odot} \text{ s}^{-1}$ is shown for presentation (note that the product $\dot{E}_{\text{iso}} \dot{M}_{\text{iso}}$ should exceed the value corresponding P_m if $\Gamma_w \sim 1$; equation 10). Three horizontal dashed lines at $\dot{E}_{\text{iso},51} = 50$, 10, and 7 are shown for illustrating purpose (arrows indicate the position where the outward shock wave is launched); Let us assume $M_{\text{ms}} = 40M_{\odot}$, $\Gamma_w \sim 1$ and $\dot{M}_{\text{iso}} = 0.1M_{\odot} \text{ s}^{-1}$. If $\dot{E}_{\text{iso},51} = 50$ or 10, the outward shock wave is launched at the intersections between the Si- and CO-layers at $M_{\text{BH}} \sim 2.4M_{\odot}$. On the other hand, if $\dot{E}_{\text{iso},51} = 7$, the momentum can not exceed the infalling ram pressure until nearly the whole CO star collapses to the central remnant at $M_{\text{BH}} \sim 13M_{\odot}$.

lows.

$$\dot{E}_w \sim A_w \Gamma_w (\Gamma_w - 1) \rho_w v_w c^2, \text{ and} \quad (8)$$

$$\dot{M}_w = A_w \Gamma_w \rho_w v_w, \quad (9)$$

where A_w is the area subtended by the wind. The asymptotic expressions for the momentum balance are derived by substituting equations (8) and (9) into equation (7);

$$\sqrt{\dot{E}_w \dot{M}_w} \equiv f_{\Omega} \sqrt{\dot{E}_{\text{iso}} \dot{M}_{\text{iso}}} \geq \frac{1}{\sqrt{2}} A_w \rho_m \bar{g} \frac{GM_{\text{BH}}}{R_w} \quad \text{for } \Gamma_w \sim 1, \quad (10)$$

$$\dot{E}_w \equiv f_{\Omega} \dot{E}_{\text{iso}} \geq c A_w \rho_m \bar{g} \frac{GM_{\text{BH}}}{R_w} \quad \text{for } \Gamma_w \gg 1. \quad (11)$$

The RHS's of equations (10) and (11), except for A_w depending on f_{Ω} , are completely determined by the progenitor structure, as a function of M_{BH} (Fig. 2). The requirement for \dot{E}_w and \dot{M}_w in terms of \dot{E}_{iso} and \dot{M}_{iso} is shown in Figure 3 as a function of M_{BH} (i.e., as a function of time). Hereafter, we use a notation $X_n \equiv X/10^n$ in CGS unit.

If $\Gamma_w \sim 1$, it is necessary that the product $\dot{E}_{\text{iso}} \dot{M}_{\text{iso}}$ should be larger than a specific value given by equation (10), which corresponds to P_m as a function of M_{BH} , in order to initiate the explosion. For $\Gamma_w \gg 1$, \dot{E}_{iso} should exceed the value given by equation (11), and the requirement becomes independent from \dot{M}_{iso} . In other ward, once the temporal evolution of \dot{E}_{iso} and \dot{M}_{iso} is given, the outward shock wave

is launched when $\dot{E}_{\text{iso}}\dot{M}_{\text{iso}}$ (or \dot{E}_{iso} if $\Gamma_w \gg 1$) is higher than the specific value representing P_m (Fig. 3).

Although P_m overall decreases as a function of M_{BH} following the density decrease, jumps are seen at the edges of the characteristic hydrostatic burning layers. Assuming freefall, $P_m \propto \rho_{\text{presn}} R_{\text{presn}}^{3/2} M_{\text{BH}}$. Within each layer, ρ_{presn} drops slowly as a function of M_{BH} and R_{presn} , making P_m nearly constant as a function of M_{BH} . On the other hand, at the edges, ρ_{presn} decreases suddenly, leading to rapidly decreasing P_m . As a result, local minimum values appear at the intersection of different layers (Fig. 3). It infers that the explosion is likely initiated at one of these intersections, but not within each layer.

This behavior of P_m provides an interesting implication. For illustration purpose, let us take the case with $M_{\text{ms}} = 40M_\odot$ and $\Gamma_w \sim 1$, assuming that $\dot{E}_{\text{iso},51}$ and \dot{M}_{iso} are constant in time. If $\dot{E}_{\text{iso},51}\dot{M}_{\text{iso},\odot} \gtrsim 1$, then the explosion is initiated below the Fe/Si interface ($M_{\text{BH}} < 2.4M_\odot$). If $0.8 < \dot{E}_{\text{iso},51}\dot{M}_{\text{iso},\odot} < 1$, the explosion position jumps to the Si/CO interface ($M_{\text{BH}} \sim 3.4M_\odot$). Then, if $\dot{E}_{\text{iso},51}\dot{M}_{\text{iso},\odot} \lesssim 0.8$, almost whole CO layer collapses onto the central remnant. Thus, we conclude that a small difference of the wind properties can lead to totally different outcome, with the critical value $\dot{E}_{\text{iso},51}\dot{M}_{\text{iso},\odot} \sim 0.8 - 1$ (for $\Gamma_w \sim 1$) or $\dot{E}_{\text{iso},51} \sim 70$ (for $\Gamma_w \gg 1$). The critical value depends on M_{ms} , and is smaller for a less massive progenitor (Fig. 3).

3.2 Production of ^{56}Ni

Once the ram pressure of the wind (P_w) overcomes the ram pressure of the infalling material (P_m), an outward shock wave is launched and explosive nucleosynthesis takes place. In this section, we examine production of ^{56}Ni as the shock wave passes through the stellar mantle (Fig. 1b). We first discuss production of ^{56}Ni in a stellar mantle heated by the shock wave (§3.2.1), then we comment on production of ^{56}Ni within the wind/jet (§3.2.2).

3.2.1 Shocked stellar mantle

The shocked mantle can become the predominant site for the ^{56}Ni synthesis, if the shock wave sweeps up a large amount of the stellar mantle, at least $\sim 0.1M_\odot$. This inevitably results in a non-relativistic shock wave, even if the wind/jet at its emergence from the central system at R_w is highly relativistic. Let us denote the average velocity and the mass of the expanding material swept up by the shock wave, by Γ_{shock} and M_{shock} , respectively, then

$$\Gamma_{\text{shock}} \sim 1 + 6 \times 10^{-4} \frac{\dot{E}_{w,51} t}{M_{\text{shock},\odot}}, \quad (12)$$

at time t (in second). In order to accelerate $\sim 0.1M_\odot$ of the stellar mantle materials to $\Gamma_{\text{shock}} = 100$, the explosion energy is required to be higher than 10^{55} ergs

We can thus use non-relativistic approximation for the postshock temperature (T) as a function of the radius of the shock wave (R_{sw}). For a radiation-dominated fireball expanding into a uniform medium with the density $\bar{\rho}$ (Maeda & Nomoto 2003),

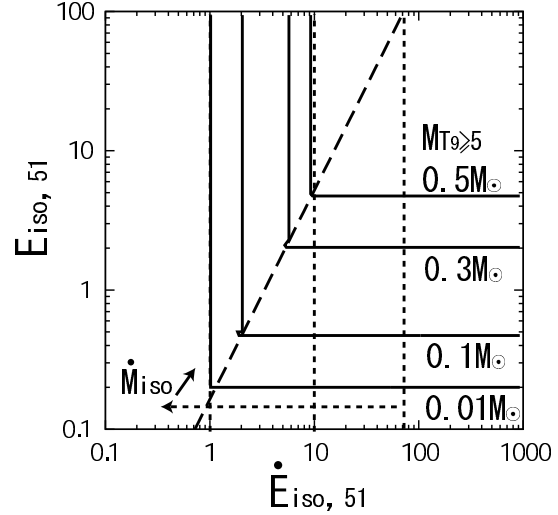


Figure 4. The isotropic mass of ^{56}Ni synthesized in the shocked stellar mantle ($M_{T_9 \geq 5}$; solid contours), for $M_{\text{BH}} = 2.4M_\odot$ and $M_{\text{ms}} = 40M_\odot$ ($13.8M_\odot$ CO star). The dashed slant line shows $\dot{E}_{\text{iso},51} = \dot{E}_{t,w,51} (E_{\text{iso}})$ as is defined by equation (14). Note that the possible value of \dot{E}_{iso} that leads to $M_{\text{BH}} = 2.4M_\odot$ is a function of \dot{M}_{iso} (see the main text). Three cases are shown for illustration, assuming the temporally constant wind injection: If $\Gamma \gg 1$, the required value for \dot{E}_{iso} is independent from \dot{M}_{iso} , and it is required that $\dot{E}_{\text{iso},51} \sim 70$ (otherwise the outward shock-wave cannot be launched at $M_{\text{BH}} = 2.4M_\odot$.) If $\Gamma_w \sim 1$, it is required that the product $\dot{E}_{\text{iso}}\dot{M}_{\text{iso}}$ should exceed a certain value, i.e., $\dot{E}_{\text{iso}}\dot{M}_{\text{iso}} \sim 1$ for the outward shock wave being launched at $M_{\text{BH}} = 2.4M_\odot$ (e.g., $\dot{E}_{\text{iso},51} \sim 10$ if $\dot{M}_{\text{iso},\odot} = 0.1$, and $\dot{E}_{\text{iso},51} \sim 1$ if $\dot{M}_{\text{iso},\odot} \sim 1$).

$$T_9 \sim \begin{cases} 5.7 \dot{E}_{\text{iso},51}^{1/6} R_{\text{sw},8}^{-1/3} \rho_6^{-1/12} & \text{for } t < t_w, \\ 24 \dot{E}_{\text{iso},52}^{1/4} R_{\text{sw},8}^{-3/4} & \text{for } t \geq t_w. \end{cases} \quad (13)$$

This expression explicitly utilizes the assumption that \dot{E}_{iso} is constant in time for $t \leq t_w$ and zero afterward.

Since M_{BH} increases monotonically with time, the density structure of the stellar mantle is specified for given M_{BH} (Fig. 2). Therefore, we can estimate the enclosed mass within a sphere in which the post-shock materials attain a certain temperature (Fig. 2; see also figure 7 of Maeda & Nomoto 2003). ^{56}Ni is synthesized in the region ($M_{T_9 \geq 5}$) where $T_9 \geq 5$. Figure 4 shows $M_{T_9 \geq 5} [= M(^{56}\text{Ni}) / f_\Omega]$; the isotropic equivalent value for $M(^{56}\text{Ni})$ for $M_{\text{BH}} = 2.4M_\odot$ and $M_{\text{ms}} = 40M_\odot$.

$M_{T_9 \geq 5}$ depends not only on E_{iso} and \dot{E}_{iso} , but also on M_{BH} . On the other hand, as concluded in §3.1, there is a condition in terms of \dot{E}_{iso} and \dot{M}_{iso} , to initiate the explosion at given M_{BH} : This indirectly relates \dot{M}_{iso} to M_{BH} . In order to obtain $M_{\text{BH}} = 2.4M_\odot$ and $M_{\text{ms}} = 40M_\odot$, it is required that $\dot{E}_{\text{iso},51}\dot{M}_{\text{iso},\odot} \gtrsim 1$ (for $\Gamma_w \sim 1$) or that $\dot{E}_{\text{iso},51} \gtrsim 70$ (for $\Gamma_w \gg 1$). Vertical dotted lines in Figure 4 explicitly describe the requirement: (1) for $\Gamma \gg 1$, $\dot{E}_{\text{iso},51} = 70$, (2) for $\Gamma \sim 1$ and $\dot{M}_{\text{iso},\odot} = 0.1$, $\dot{E}_{\text{iso},51} = 10$, and (3) for $\Gamma \sim 1$ and $\dot{M}_{\text{iso},\odot} = 1$, $\dot{E}_{\text{iso},51} = 1$.

Interestingly, the dependence of $M(^{56}\text{Ni})$ on \dot{E}_{iso} and E_{iso} (Fig. 4) changes the behavior at a specific slant line in the $\dot{E}_{\text{iso}} - E_{\text{iso}}$ plane. The line is obtained by equalizing the two RHS's of equations (13) and defined as

$$\dot{E}_{t_w,51}(E_{\text{iso}}) \equiv \left(\frac{2.9}{T_9}\right)^{-10/3} \bar{\rho}_6^{-1/2} E_{\text{iso},51}^{2/3}, \quad (14)$$

with $T_9 = 5$, i.e., the temperature necessary for the production of ^{56}Ni . For given E_{iso} , $M(^{56}\text{Ni})$ is larger for larger \dot{E}_{iso} as long as $\dot{E}_{\text{iso}} \leq \dot{E}_{t_w}$, but saturated for $\dot{E}_{\text{iso}} > \dot{E}_{t_w}$.

The dividing energy injection rate, $\dot{E}_{t_w}(E_{\text{iso}})$, appears, because of the different behavior of the post-shock temperature before and after $t = t_w$ (Maeda 2004). The mass of ^{56}Ni is determined by the radius of the outward shock wave when the temperature drops down to $T_9 = 5$. If $\dot{E}_{\text{iso}} \leq \dot{E}_{t_w}$ (for given E_{iso}), then the temperature behind the shock wave drops down to $T_9 = 5$ during the phase when the energy source is still active (i.e., $t < t_w$). Thus, larger \dot{E}_{iso} corresponds to the larger amount of energy contained behind the shock wave, leading to the larger radius of the shock wave when the condition $T_9 = 5$ is satisfied (e.g., see Fig. 2). On the other hand, the condition $\dot{E}_{\text{iso}} > \dot{E}_{t_w}$ corresponds to the case in which all the energy from the central source is liberated in short time scale such that the temperature is still high ($T_9 > 5$) at $t = t_w$. The following evolution of the shock wave, which determines $M_{T_9 \geq 5}$, is controlled by E_{iso} , not by \dot{E}_{iso} .

It has been suggested that $M(^{56}\text{Ni})$ is larger for larger E_{iso} (e.g., Nakamura et al. 2001b), but this holds true only if the energy is generated and liberated almost promptly (i.e., $t_w \rightarrow 0$ and $\dot{E}_{\text{iso}} \rightarrow \infty$). For example, if $\dot{E}_{\text{iso},51} = 1$, then $M(^{56}\text{Ni})$ does not depend on the total energy E_{iso} (or E_w) (as long as $E_{\text{iso},51} \gtrsim 0.2$) (Fig. 4).

3.2.2 ^{56}Ni in the wind/jet

Mass of the wind is

$$M_w = \frac{\dot{M}_w}{\dot{E}_w} E_w \sim \frac{E_w}{c^2(\Gamma_w - 1)}, \quad (15)$$

which must be smaller than the mass of the accreted materials, i.e., $M_w < M_{\text{BH}} - 1.4M_\odot$. Composition of the materials within the disk wind is largely uncertain, because it depends on the thermal history of the wind in the vicinity of the central remnant (i.e., well below R_w). The deep understanding of the composition of the wind material requires numerical calculations or analytic investigation of the innermost part of the collapsing star (e.g., MacFadyen & Woosley 1999; Pruet, Thompson, & Hoffman 2004; Nagataki et al. 2007).

However, it is still possible to make a rough estimate, in order to see in what regions in the $\dot{E}_{\text{iso}} - \dot{M}_{\text{iso}}$ plane the disk wind is important. Assuming that the energy of the wind is initially thermal energy-dominated near the central remnant, the typical entropy of the wind material $s \equiv S/(k_B/m_u)$ (where k_B and m_u are the Boltzmann constant and atomic unit mass, respectively) is written by \dot{E}_{iso} and \dot{M}_{iso} as follows:

$$s \sim \begin{cases} 22(\dot{E}_{\text{iso},51} \dot{M}_{\text{iso},\odot})^{3/8} & \text{for } \Gamma_w \sim 1, \\ 11\dot{E}_{\text{iso},52}^{3/4} & \text{for } \Gamma_w \gg 1. \end{cases} \quad (16)$$

We find that $s \gg 1$ in the parameter range of our interest; s can be as small as about unity, only when either $\dot{E}_{\text{iso}} \dot{M}_{\text{iso}}$ or \dot{E}_{iso} is very small, but in such a case the whole star collapses onto the central remnant (§3.1). Thus, when \dot{E}_{iso} and \dot{M}_{iso} are large enough to result in a supernova explosion, the wind material should experience the strong

α -rich freezeout, leaving mainly ^4He , not ^{56}Ni . The strong α -rich freezeout is consistent with numerical calculations of the collapsing star (Nagataki et al. 2007). In what follows, we take $M(^{56}\text{Ni}) = 0.2M_w$ in the wind which is typical for the strong α -rich freezeout (e.g., Pruet et al. 2004; but see §5 for further discussion on the uncertainty).

3.3 Geometry of the ejecta

The geometry of the bulk supernova materials provide a useful constraint on the model, since recently more and more observational data have been available to address the ejecta geometry (see Wang & Wheeler 2008 for a review of spectropolarimetry; for recent spectroscopy, see Maeda et al. 2008; Modjaz et al. 2008). Here we give a rough estimate of how the geometry depends on the wind parameters. Note that the geometry of the bulk supernova materials is different from the geometry of the wind at the injection measured by f_Ω ; Even if the wind is initially collimated ($f_\Omega < 1$), the bulk expansion of the stellar mantle, as is induced by the wind, can be less collimated or even quasi-spherical.

The shock breakout time (t_{sb}) of the wind/jet is estimated by

$$t_{\text{sb}} \sim R_{\text{CO}}/v_{\text{shock}}, \quad (17)$$

$$v_{\text{shock}} \equiv \left(\frac{2\dot{E}_{\text{iso}} t_{\text{sb}}}{(M_{\text{CO}} - M_{\text{BH}})} \right)^{1/2}. \quad (18)$$

Here R_{CO} and M_{CO} are the radius and the mass of the CO star. For $M_{\text{ms}} = 40M_\odot$, these values are $R_{\text{CO}} \sim 10^{10}$ cm and $M_{\text{CO}} \sim 13.8M_\odot$.

As the wind/jet pushes the stellar mantle, the wind/jet loses its energy by depositing its energy into the surroundings. If the energy injection is terminated before it breaks through the progenitor surface (R_{CO}), a large fraction of the energy of the wind/jet are transferred to the stellar mantle. This results in a quasi-spherical explosion of the bulk of the stellar mantle, even if the wind/jet is initially collimated. This happens if the following condition is satisfied.

$$t_w \sim \frac{E_{\text{iso}}}{\dot{E}_{\text{iso}}} < t_{\text{sb}} \sim \left(\frac{R_{\text{CO}}^2 (M_{\text{CO}} - M_{\text{BH}})}{2\dot{E}_{\text{iso}}} \right)^{1/3}. \quad (19)$$

On the other hand, if $t_w > t_{\text{sb}}$, then a large amount of materials are ejected toward the jet direction as compared to the equatorial direction, resulting in a strongly jetted explosion.

4 COMPARISON TO OBSERVATIONS

The expected SN properties can be expressed by \dot{E}_{iso} and \dot{M}_{iso} and the temporal evolution of these, once the other parameters are specified (M_{ms} , E_{iso} or E_w , and f_Ω). For comparison to the observation presented below, we examine the simplest case, in which \dot{E}_{iso} and \dot{M}_{iso} are constant in time for $t < t_w$ and zero afterward (i.e., $E_{\text{iso}} = \dot{E}_{\text{iso}} t_w$). This is a situation examined in most of the previous numerical studies, except for MacFadyen et al. (2001) and Maeda & Nomoto (2003) who examined the case where the energy injected by the jet (wind) is connected to the accretion rate to the central remnant.

First, the momentum balance determines when the outward shock wave is launched, yielding M_{BH} at this time as

a function of \dot{E}_{iso} and \dot{M}_{iso} (§3.1; Figure 3). Then, the analysis presented in §3.2.1 gives us the mass of ^{56}Ni , as this is given as a function of M_{BH} , \dot{E}_{iso} , and E_{iso} (Figure 4). The mass of ^{56}Ni in the disk can be roughly evaluated using the result of §3.2.2 (equation 15). Finally, the typical geometrical feature can be derived as a function of \dot{E}_{iso} , E_{iso} , M_{BH} (§3.3; equation 19).

Using the expressions derived in §3, we characterize properties of a SN explosion as a function of \dot{E}_{iso} and \dot{M}_{iso} for a given progenitor model (M_{ms}). Other parameters are f_{Ω} , E_w (or t_w), but these can be set without large ambiguity by observations for some GRB-SNe of special interest.

4.1 SN 1998bw: the origin of ^{56}Ni

SN Ic 1998bw is a prototypical SN associated with a GRB. For SN 1998bw, intensive observational data in the optical wavelength are available: modeling these observations (by one-dimensional radiation transfer calculations; Iwamoto et al. 1998; Woosley et al. 1999; Nakamura et al. 2001a) suggests that $E_{\text{iso}} \sim 30$ and $M_{\text{ms}} \sim 40M_{\odot}$. Adding to this, there exists intensive study for this object using multi-dimensional radiation transfer calculations (Maeda 2006a; Maeda et al. 2006b; Tanaka et al. 2007). The study suggests that the intrinsic explosion energy is smaller than the isotropic value by a factor of about 3, inferring that $f_{\Omega} \sim 0.3$ is a good approximation.

Figure 5a shows the result for $E_{\text{iso},51} = 30$, $f_{\Omega} = 0.3$, and $M_{\text{ms}} = 40M_{\odot}$. Here, we try to constrain the properties of the wind generated by the activity of the central engine of SN 1998bw, i.e., \dot{E}_{iso} and \dot{M}_{iso} (or equivalently, \dot{E}_w and \dot{M}_w). For SN 1998bw, observations constrain three quantities, the ejecta mass, $M(^{56}\text{Ni})$, and the shape of the ejecta: (1) The ejecta contain a large amount of the CO-core materials, so that $M_{\text{BH}} < 10M_{\odot}$, as inferred by the optical light curve and spectra (§3.1). (2) $M(^{56}\text{Ni}) \sim 0.4M_{\odot}$ to explain its peak luminosity (§3.2). (3) The ejecta are suggested to be aspherical, but still a large amount of materials are ejected into the equatorial direction as inferred especially by spectra at ~ 1 year since the explosion (Patat et al. 2001; Mazzali et al. 2001; Maeda et al. 2002). This indicates that the expanding supernova ejecta are quasi-spherical, rather than extremely bipolar (§3.3)

The three conditions are simultaneously satisfied if $\dot{E}_{\text{iso},51}\dot{M}_{\text{iso},\odot} \gtrsim 1$ and $\dot{E}_{\text{iso},51} \gtrsim 20$ (for $\Gamma_w \sim 1$), or $\dot{E}_{\text{iso},51} > 70$ (for $\Gamma_w \gg 1$) (region A in Figure 5b). In these cases, ^{56}Ni is predominantly produced at the shocked stellar mantles. The wind origin for ^{56}Ni is disfavored for SN 1998bw. The wind contribution exceeds the shocked mantle contribution only if $\dot{E}_{\text{iso},51} \lesssim 5$ and $\dot{M}_{\text{iso},\odot} \gtrsim 0.2$ (i.e., region C of Figure 5b). However, this combination of the parameters results in $t_w/t_{\text{sb}} > 1$ and an essentially bipolar explosion, as is inconsistent with the observation.

In short, the wind should be massive and long-lived (i.e., large \dot{M}_{iso} and large t_w ; see equation 15), in order to produce a large amount of ^{56}Ni within the wind (as large as $\sim 0.4M_{\odot}$). However, such an explosion with a long-lived energy injection results in the extremely bipolar explosion, since the outward shock wave can reach the stellar surface before the energy injection is terminated: This argues against the wind-origin of ^{56}Ni in SN 1998bw.

4.2 Diversity of GRB-SNe

Figure 5b shows the expected characteristics of GRB-SNe for $E_{\text{iso}} = 30$, $f_{\Omega} = 0.3$, and $M_{\text{ms}} = 40M_{\odot}$. A variety of features are predicted for the wind-driven supernovae depending on \dot{E}_{iso} and \dot{M}_{iso} .

If $\dot{E}_{\text{iso},51}\dot{M}_{\text{iso},\odot} \gtrsim 1$ ($\Gamma_w \sim 1$) or $\dot{E}_{\text{iso},51} \gtrsim 70$ ($\Gamma_w \gg 1$), then the resulting SNe should be similar to SN 1998bw in the ejected mass. The features are further divided as follows (regions A, B, and C in Figure 5b):

(A) SN 1998bw-like – GRB-SNe 1998bw, 2003dh, and 2003lw: In the parameter region A, the wind-driven supernova is similar to GRB-SN 1998bw, in virtually all the observed characteristics. The luminosity is similar to that of SN 1998bw, since $M(^{56}\text{Ni}) \sim 0.3 - 0.6M_{\odot}$.

This category can account for GRB-SNe 1998bw, 2003dh, and 2003lw. The region is relatively large in terms of \dot{E}_{iso} and \dot{M}_{iso} , and the features of supernovae are insensitive to \dot{E}_{iso} and \dot{M}_{iso} ; This can explain why these three GRB-SNe are similar in the optical properties.

(B) Sub-luminous SN 1998bw-like – GRBs 040924 and 041006?: In the parameter region B, the expected supernovae are similar to SN 1998bw in the ejected mass and the geometry, but the difference is seen in $M(^{56}\text{Ni})$. This indicates that the supernovae has similar optical properties with SN 1998bw, with the diversity in the luminosity, covering $\sim 0.3 - 1$ times that of SN 1998bw. This diversity arises because, in this parameter region, \dot{E}_{iso} is smaller than \dot{E}_{t_w} , and thus $M(^{56}\text{Ni})$ is dependent on \dot{E}_{iso} (§3.2.1) [note that \dot{E}_{iso} is larger than \dot{E}_{t_w} in region A, and thus $M(^{56}\text{Ni})$ is independent from \dot{E}_{iso} unlike region B]. This parameter region B can account for sub-luminous SNe found as bumps in optical afterglows of some GRBs (e.g., GRBs 040924 and 041006).

(C) Bipolar SN 1998bw-like: In the parameter region C, a resulting SN is similar to SN 1998bw in its luminosity and ejecta mass, but the ejecta are more highly beamed than SN 1998bw. We have never directly observed such peculiar GRB-SNe. If such a GRB-SN is observed in future, it will provide a strong evidence of the diverse property of the central engine, in terms of \dot{E}_{iso} and \dot{M}_{iso} .

Here, ^{56}Ni is mainly produced within the wind materials. The bipolar explosion results from the central energy source being active for a long time period (c.f., equation 19; e.g., low \dot{E}_{iso} smaller than \dot{E}_w). As such, (1) the mass of ^{56}Ni produced within the shocked stellar mantle is small, and (2) the wind should be massive to initiate the explosion (to provide the sufficiently large momentum in the non-relativistic regime). As a result, the wind contribution dominates over the shocked stellar mantle in the production of ^{56}Ni for the (extremely) bipolar explosion case.

If $\dot{E}_{\text{iso},51}\dot{M}_{\text{iso},\odot} \lesssim 1$ ($\Gamma_w \sim 1$) or $\dot{E}_{\text{iso},51} \lesssim 70$ ($\Gamma_w \gg 1$), then the resulting SNe should intrinsically different from SN 1998bw in the ejected mass (§3.1; regions D and E in Figure 5b). At the low end of \dot{E}_{iso} or \dot{M}_{iso} , a supernova can never be triggered.

(D) Bipolar SN with the ejected mass $\lesssim 1M_{\odot}$ – GRBs 060505 and 060614?: In the parameter region D, only a small amount of materials ($< 1M_{\odot}$) near the surface of the CO layer are ejected. The supernova ejecta are essentially bipolar in this case. ^{56}Ni is mainly originated in

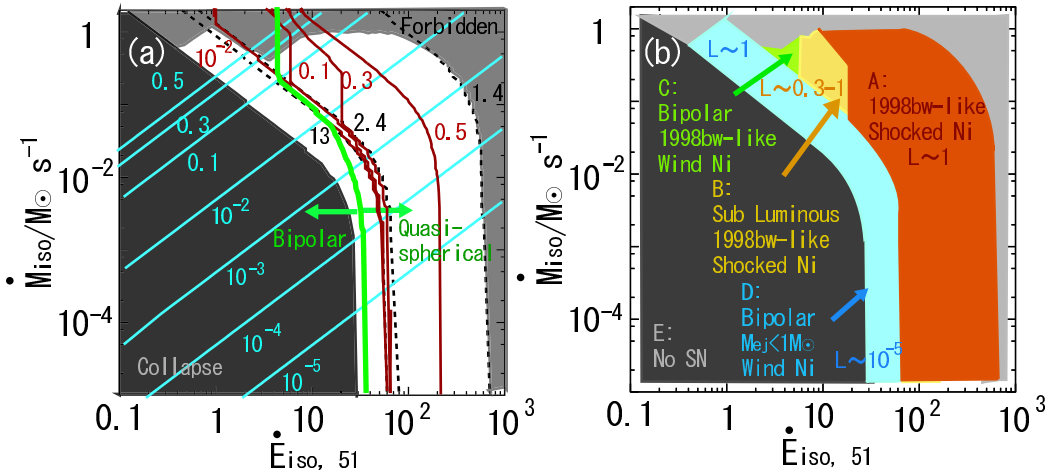


Figure 5. (a) Estimate of $M(^{56}\text{Ni})$ in the $\dot{E}_{\text{iso}} - \dot{M}_{\text{iso}}$ plane. The progenitor is the $13.8M_{\odot}$ CO star ($M_{\text{ms}} = 40M_{\odot}$), taken from Nomoto & Hashimoto (1988). The other two parameters are set as $E_{\text{iso},51} = 30$ and $f_{\Omega} = 0.3$, representing the bright GRB-SN 1998bw. $M(^{56}\text{Ni})/M_{\odot}$ is shown for the shocked stellar mantle (red contours) and the wind (blue contours). M_{BH}/M_{\odot} is shown by the black-dotted contours. The shaded region denoted by "Forbidden" is excluded by the requirement that the ejected mass must not exceed the available accreted mass budget. The dark shaded region denoted by "Collapse" corresponds to whole collapse of the CO star. The green curve shows the line where $t_w \sim t_{\text{sb}}$. (b) Expected characteristics of GRB-SNe for $M_{\text{ms}} = 40M_{\odot}$. In each region, "L" denote a rough estimate of the SN peak luminosity normalized by that of SN 1998bw.

the wind. Thus, $M(^{56}\text{Ni}) \propto \dot{M}_w/\dot{E}_w$, ranging from $M(^{56}\text{Ni}) < 10^{-5}M_{\odot}$ to $\sim 0.3M_{\odot}$. The expected luminosity is thus diverse, depending on \dot{E}_{iso} and \dot{M}_{iso} . This may correspond to non-detection of supernova features in GRBs 060505 and 060614 (which may also be explained by region E below).

(E) No supernova – GRBs 060505 and 060614?: In the parameter region E, the wind injection can never set the outward shock wave. This case corresponds to whole collapse of the progenitor CO star without a SN.

5 CONCLUSIONS AND DISCUSSION

In this paper, we discussed theoretically expected characteristics of a supernova driven by the wind/jet. We found that the resulting supernova features can be categorized as a function of \dot{E}_{iso} and \dot{M}_{iso} . Thus, it is possible to constrain the nature of the central engine of GRBs by observations of associated supernovae.

Results of the past numerical studies can be understood as a limiting case. For example, Nakamura et al. (2001b) showed that $M(^{56}\text{Ni})$ is larger for larger E_{iso} . In this paper, we have clarified that it holds true only for the limiting case where $t_w \rightarrow 0$ and thus $\dot{E}_{\text{iso}} \rightarrow \infty$. For another example, Tominaga et al. (2007b) showed that \dot{E}_{iso} determines $M(^{56}\text{Ni})$. In this paper, we have shown that this behavior appears as a limiting case where $\Gamma \gg 1$, and the dependence is different when $\Gamma \sim 1$.

For SN 1998bw, we find that observations are reproduced only if $\dot{E}_{\text{iso},51}\dot{M}_{\text{iso},\odot} \gtrsim 1$ and $\dot{E}_{\text{iso},51} \gtrsim 20$ (if $\Gamma_w \sim 1$), or $\dot{E}_{\text{iso},51} \gtrsim 70$ (if $\Gamma_w \gg 1$) (region A in Fig. 5 b). We favor the shocked stellar mantle as the main site of the production of ^{56}Ni .

Furthermore, the observed diversity of supernovae associated (or not associated) with GRBs can be accounted for by the diverse properties of the wind from the central remnant (\dot{E}_{iso} and \dot{M}_{iso}). It is shown that the different wind

properties can potentially explain the diversity of supernovae associated with GRBs.

Further diversity can arise from different progenitors (M_{ms}). Irrespective of M_{ms} , the expected features of the wind-driven supernovae can be categorized as we did for $M_{\text{ms}} = 40M_{\odot}$ (§4), i.e., regions A – E. The positions of the boundaries between different regions, as well as maximum $M(^{56}\text{Ni})$ at the high end of \dot{E}_{iso} and \dot{M}_{iso} , are dependent on M_{ms} . For $M_{\text{ms}} = 25M_{\odot}$, the boundary between regions A and D is located at $\dot{E}_{\text{iso},51}\dot{M}_{\text{iso},\odot} \sim 0.05$ (for $\Gamma_w \sim 1$) or $\dot{E}_{\text{iso},51} \sim 20$ (for $\Gamma_w \gg 1$), smaller than for $M_{\text{ms}} = 40M_{\odot}$ by about one order of magnitude (Fig. 3). Using $f_{\Omega} = 0.3$ and $E_{\text{iso},51} = 30$, maximum $M(^{56}\text{Ni})$ is $\sim 0.24M_{\odot}$ even if $M_{\text{BH}} = 1.4M_{\odot}$. Thus, $M_{\text{ms}} = 25M_{\odot}$ never yield bright SN 1998bw-like SNe. We therefore confirmed that the prototypical GRB-SN 1998bw and the similar SNe 2003dh and 2003lw must have originated from a massive progenitor ($M_{\text{ms}} \sim 40M_{\odot}$) from the nucleosynthesis argument.

Also, the diversity arising from M_{ms} may be important to explain the sub-luminous supernovae possibly associated with GRBs 040924 and 041006. These can be explained by $M_{\text{ms}} \sim 40M_{\odot}$ with smaller \dot{E}_{iso} and \dot{M}_{iso} than for SN 1998bw. Alternatively, it is also possible that the central engine provides \dot{E}_{iso} and \dot{M}_{iso} similar to SN 1998bw, but the progenitor mass is smaller than SN 1998bw (i.e., region A for $M_{\text{ms}} = 25M_{\odot}$). It is thus important to derive M_{ms} for these sub-luminous cases, by spectroscopic and light curve modeling, to distinguish these possibilities.

On the other hand, the diversity in terms of M_{ms} is not important in interpreting no detection of supernovae associated with GRBs 060505 and 060614. If they are the outcome of the core collapse of a massive star, the properties of the wind/jet should fall in the low end of \dot{E}_w and \dot{M}_w (region E), or region D with $\dot{M}_{\text{iso},\odot} \lesssim 10^{-3}$. If this is not the case, we should have detected associated supernovae. Note that Tominaga et al. (2007b) showed that the wind/jet-driven explosion with small \dot{E}_{iso} "can" account for the non-

detection of supernovae in these GRBs, while this study has shown that \dot{E}_{iso} and/or \dot{M}_{iso} "must" be small in the central engine of these GRBs. These GRBs highlight our suggestion that we can constrain the properties of the central engine by observations (non-detection, in this case) of associated supernovae.

The present analysis is based on one-dimensional calculations. We predict that the different categories (A–E) are divided rather sharply in terms of \dot{M}_{iso} and \dot{E}_{iso} , while in reality this may well be smoothed by the jet-accretion interaction (Maeda & Nomoto 2003; Tominaga et al. 2007). Although the jet-accretion interaction should create a non-radial flow, key conclusions in the present paper are not defeated. For example, our model can explain the qualitative behaviors found in the past numerical study, and can reach at least rough quantitative agreement for the important quantity like $M(^{56}\text{Ni})$ (for limited parameter space as investigated by numerical study; see also Maeda & Nomoto 2003).

The largest uncertainty involved in the present analysis is in the treatment of nucleosynthesis within the wind material, specifically, the assumption that 20% of the wind materials become ^{56}Ni . Surman, McLaughlin, & Hix (2006) concluded that the ^{56}Ni mass fraction could be as large as $\sim 50\%$ for the wind/jet with the entropy in the range between 10 and 30. This does not affect our conclusion for $\Gamma_w \gg 1$, as the mass of the wind materials is anyway small in this case. The only conclusion possibly affected by this uncertainty is the supernova feature in the region B. From equation 16, we see that the entropy of the wind materials falls into the range $s = 10 - 30$ if $\dot{E}_{\text{iso},51} \dot{M}_{\text{iso},\odot} \sim 1$. This line crosses the vicinity of region B, and lead to the contribution of the wind materials for the ^{56}Ni production comparable to that of the shocked mantle in this region. As such, $M(^{56}\text{Ni})$ in this region may have a significant contribution from the wind materials.

ACKNOWLEDGMENTS

This research has been supported by World Premier International Research Center Initiative (WPI Initiative), MEXT, Japan, and partly by the Grant-in-Aid for Young Scientists of the JSPS/MEXT (20840007). N.T. is supported by the JSPS postdoctoral fellowship. The authors would like to thank Ken'ichi Nomoto, Hideyuki Umeda, Masaru Shibata, and Yuichiro Sekiguchi for useful discussion.

REFERENCES

Brown G.E., Lee, C.-H., Wijers R.A.M.J., Lee H.K. Israelian G. Bethe H.A. 2000, *New Astronomy*, 5, 191
 Della Valle M., et al. 2006, *Nature*, 444, 1050
 Della Valle M., et al. 2008, *CBET*, 1602
 Fryer C.L., Mészáros P. 2003, *ApJ*, 588, L25
 Fynbo J.P.U., et al. 2006, *Nature*, 444, 1047
 Galama T.J., et al. 1998, *Nature*, 395, 670
 Gal-Yam A., et al. 2006, *Nature*, 444, 1053
 Hjorth J., Holland S., Courbin F., Dar A., Olsen L.F., Scodreggio M. 2000, *ApJ*, 534, L147
 Hjorth J., et al. 2003, *Nature*, 423, 847

Iwamoto K., et al. 1998, *Nature*, 395, 672
 Kawabata K. et al. 2003, *ApJ*, 593, L19
 Khokhlov A.M., Höflich P.A., Oran E.S., Wheeler, J.C., Wang L., Chtchelkanova A. Yu. 1999, *ApJ*, 524, L107
 MacFadyen A. I., Woosley S. E. 1999, *ApJ*, 524, 262
 MacFadyen A. I., Woosley S. E., Heger A. 2001, *ApJ*, 550, 410
 Maeda K. 2004, Ph. D. Thesis, University of Tokyo
 Maeda K. 2006a, *ApJ*, 644, 385
 Maeda K., Nomoto K., 2003, *ApJ*, 598, 1163
 Maeda K., Nakamura T., Nomoto K., Mazzali P.A., Patat F., Hachisu I. 2002, *ApJ*, 565, 405
 Maeda K., Mazzali P.A., Nomoto K. 2006b, *ApJ*, 645, 1331
 Maeda K., Nomoto K., Mazzali P.A., Deng J. 2006c, *ApJ*, 640, 854
 Maeda, K. et al. 2008, *Science*, 319, 1220
 Malesani D., et al. 2004, *ApJ*, 609, L5
 Matheson T., et al. 2003, *ApJ*, 599, 394
 Mazzali P.A., Nomoto K., Patat F., Maeda K. 2001, *ApJ*, 559, 1047
 Mazzali P.A., et al. 2003, *ApJ*, 599, L95
 Mazzali P.A., et al. 2006, *ApJ*, 645, 1323
 Modjaz M., Kirshner R.P., Blondin S., Challis P., Matheson T. 2008, *ApJ*, 687, L9
 Nakamura T., Mazzali P.A., Nomoto K., Iwamoto K. 2001a, *ApJ*, 550, 991
 Nakamura T., Umeda H., Iwamoto K., Nomoto K., Hashimoto M., Hix W.R., Thielemann F.-K. 2001b, *ApJ*, 555, 880
 Nagataki S., Mizuta A., Yamada S., Takabe H., Sato K. 2003, *ApJ*, 596, 401
 Nagataki S., Mizuta A., & Sato K. 2006, *ApJ*, 647, 1255
 Nagataki S., Takahashi R., Mizuta A., Takiwaki T. 2007, *ApJ*, 659, 512
 Narayan R., Piran T., Kumar P. 2001, *ApJ*, 557, 949
 Nomoto K., Hashimoto M., 1988, *Phys. Rep.* 163, 13
 Nomoto K., Tominaga N., Tanaka M., Maeda K., Suzuki T., Deng J.S., Mazzali P.A. 2007, *SWIFT and GRBs: Unveiling the Relativistic Universe*, II *Nuovo Cimento*, in press (astro-ph/0702472)
 Patat, F. et al. 2001, *ApJ*, 555, 900
 Price P.A., et al. 2003, *ApJ*, 584, 931
 Proga D., MacFadyen A.I., Armitage P.J., Begelman M.C. 2003, *ApJ*, 599, L5
 Pruet J., Thompson T.A., Hoffman R.D. 2004, *ApJ*, 606, 1006
 Soderberg A.M., et al. 2006, *ApJ*, 636, 391
 Soderberg A.M., et al. 2008, *GCN Circ.*, 8662
 Stanek K. Z., et al. 2003, *ApJ*, 591, L17
 Surman R., McLaughlin, G.C., Hix W.R. 2006, *ApJ*, 643, 1057
 Tanaka M., Maeda K., Mazzali P.A., Nomoto K. 2007, *ApJ*, 668, L19
 Thomsen B., et al. 2004, *A&A*, 419, L21
 Tominaga N. 2007a, Ph. D. Thesis, University of Tokyo
 Tominaga N. 2009, *ApJ*, 690, 526
 Tominaga N., Maeda K., Umeda H., Nomoto K., Tanaka M., Iwamoto N., Suzuki T., Mazzali P.A. 2007b, *ApJ*, 657, L77
 Wang L., Wheeler J.C. 2008, *ARAA*, 46, 433
 Woosley S.E. 1993, *ApJ*, 405, 273
 Woosley S.E., Bloom J.S. 2006, *ARAA*, 44, 507

Woosley S.E., Eastman E.G., Schmidt B.P. 1999, ApJ, 516,
788

Zeh A., Klose S., Hartmann D.H. 2004, ApJ, 609, 952

This paper has been typeset from a \TeX / \LaTeX file prepared
by the author.